SANDIA REPORT
SAND88—1249 • UC—236
Unlimited Release
Printed July 1988

Analysis of Steam Injected Gas Turbines for Solar Thermal Applications

Kevin L. Linker

Prepared by
Sandia National Laboratories
Albuquerque, New Mexico 87185 and Livermore, California 94550
for the United States Department of Energy
under Contract DE-AC04-76DP00789

Issued by Sandia National Laboratories, operated for the United States Department of Energy by Sandia Corporation.

Printed in the United States of America
Available from
National Technical Information Service
U.S. Department of Commerce
5285 Port Royal Road
Springfield, VA 22161

NTIS price codes
Printed copy: A03
Microfiche copy: A01

SAND88-1249
Unlimited Release

Distribution
Category UC-236

ANALYSIS OF STEAM INJECTED GAS TURBINES FOR SOLAR THERMAL APPLICATIONS*

Kevin L. Linker
Solar Distributed Receiver Division
Sandia National Laboratories
Albuquerque, New Mexico

ABSTRACT

The Department of Energy's (DOE) Solar Thermal Program has as one of its program elements the development and evaluation of heat engine technologies that are applicable to Distributed Receiver Systems. The primary research and development activities, for the past several years, have involved the dish-electric concept in which a heat engine, solar receiver, and generator are combined as a power conversion assembly (PCA) and mounted at the focus of a parabolic dish concentrator. PCAs based on Rankine, Brayton, and Stirling cycle heat engines have been designed and built at 10-25 kWe power levels with varying degrees of success. The small Brayton cycle engines in particular have fallen short of expectations as a focal mounted PCA. This report analyzes larger Brayton engines (500 kWe and above) supplied with fossil fuel and solar energy from 15-m diameter parabolic dishes or small central receivers. In particular, a steam injected gas turbine (STIG) cycle is examined because of its ability to offer higher efficiencies as compared to the combined cycle, regenerative Brayton cycle, and water injected Brayton cycle. This report outlines quantitatively the cycle parameters that affect efficiency for a solar-augmented steam-injected gas turbine.

---

*This work was supported by the U.S. Department of Energy (U.S. DOE) under Contract DE-AC04-76DP00789.

TABLE OF CONTENTS

	Page
1. Introduction	1
2. Regenerative Gas Turbine Cycle	1
3. Combined Cycle	2
4. Water Injected Gas Turbine Cycle	3
5. Steam Injected Gas Turbine Cycle	4
6. Analysis of Steam Injected Gas for Solar Application	6
7. Solar Receiver Analysis	12
8. Results	15
9. Conclusions	19
References	21
Appendix A (Nomenclature)	22

FIGURES & TABLES

Fig.		Page
1.	Regenerative Gas Turbine Cycle	2
2.	Combined Cycle	3
3.	Water Injected Gas Turbine	4
4.	Steam Injected Gas Turbine	5
5.	Closed STIG Cycle	5
6.	Steam Injected Cycle with Parabolic Dish Concentrator	6
7.	Steam Injected Cycle with Central Receiver	7
8.	STIG Cycle	7
9.	Temperature-Entropy Diagram	8
10.	Temperature Distribution in HRSG	11
11.	Cavity Receiver/Parabolic Concentrator	12
12.	Receiver Efficiency vs Insolation and T_{rs}	15
13.	3-D Surface at Constant PR	16
14.	3-D Surface at Constant TIT	16
15.	STIG Cycle Efficiency vs X	17
16.	Temperature/Quality/η vs X	18
17.	Actual T_p vs Design T_p	18
18.	Solar System Efficiency vs TIT and PR	19

TABLES

Tables	Page
1. Receiver - Concentrator Parameters	14
2. Cycle Parameters	15

SOLAR THERMAL TECHNOLOGY

FOREWORD

The research and development described in this document was conducted within the U.S. Department of Energy's (DOE) Solar Thermal Technology Program. The goal of the Solar Thermal Technology Program is to advance the engineering and scientific understanding of solar thermal technology and to establish the technology base from which private industry can develop solar thermal power production options for introduction into the competitive energy market.

Solar thermal technology concentrates solar radiation by means of tracking mirrors or lenses onto a receiver where the solar energy is absorbed as heat and converted into electricity or incorporated into products as process heat. The two primary solar thermal technologies, central receivers and distributed receivers, employ various point and line-focus optics to concentrate sunlight. Current central receiver systems use fields of heliostats (two-axis tracking mirrors) to focus the sun's radiant energy onto a single tower-mounted receiver. Parabolic dishes up to 17 meters in diameter track the sun in two axes and use mirrors to focus radiant energy onto a receiver. Troughs are line-focus tracking reflectors that concentrate sunlight onto receiver tubes along their focal lines. Concentrating collector modules can be used alone or in a multi-module system. The concentrated radiant energy absorbed by the solar thermal receiver is transported to the conversion process by a circulating working fluid. Receiver temperatures range from 100°C in low-temperature troughs to over 1500°C in dish and central receiver systems.

The Solar Thermal Technology Program is directing efforts to advance and improve promising system concepts through the research and development of solar thermal materials, components, and subsystems, and the testing and performance evaluation of subsystems and systems. These efforts are carried out through the technical direction of DOE and its network of national laboratories who work with private industry. Together they have established a comprehensive, goal directed program to improve performance and provide technically proven options for eventual incorporation into the Nation's energy supply.

To be successful in contributing to an adequate national energy supply at reasonable cost, solar thermal energy must eventually be economically competitive with a variety of other energy sources. Components and system-level performance targets have been developed as quantitative program goals. The performance targets are used in planning research and development activities, measuring progress, assessing alternative technology options, and making optimal component developments. These targets will be pursued vigorously to insure a successful program.

This report presents a heat engine cycle for solar thermal applications which could meet DOE's near-term and long-term goals. Development cost and proof-of-concept would not solely burden the Solar Thermal Technology Program. Its application is becoming wide spread throughout the power generating industry.

1. INTRODUCTION

Gas turbine technology offers several advantages for solar applications. Gas turbines or Brayton cycles have grown from a level of understanding beginning in 1791 when the first patent was issued for a gas turbine engine [1]. Major breakthroughs are not required to adapt this technology to solar use. The gas turbine is inherently simple because it has only two rotating parts and essentially no heat exchangers. Manufacture, construction, and maintenance are relatively easy. Gas turbines have demonstrated hundreds of thousands of hours of operation and a large infrastructure exists to maintain these machines. Gas turbines can have high cycle efficiencies and high specific power. For solar applications this could be a major advantage. When incorporated in a hybrid solar system the gas turbine offers the distinct advantage of internal combustion; a heat exchanger is not required to transfer energy into the engine. The addition of a direct absorption solar receiver can be a simple matter for a gas turbine. Sanders Associates demonstrated this concept with their Development Test Module [2]. Finally, gas turbines are readily available from several manufactuers in larger ouput sizes making near-term delivery and installation of a gas turbine for solar applications practical.

The use of steam injected gas turbines (STIG) for power generation has long been recognized. However, results in many instances have been disappointing in terms of system efficiencies. The steam injected cycle is a combination of Brayton and Rankine cycles. The working fluid for each cycle is compressed separately, heated, and then combined for expansion and heat rejection. The two fluid streams are then separated by condensing the Rankine fluid. The use of two fluids, two thermodynamic cycles, and the operating parameters that maximize the system efficiency for a steam injected gas turbine (STIG) cycle is a patented cycle known as the Parallel-Compound Dual Fluid Heat Engine or the Cheng cycle [3].

The STIG cycle differs from the regenerative cycle, combined cycle, and water injected gas turbine cycle in several ways. Each of these cycles is briefly outlined, together with its differences from the steam injected cycle. The STIG is then analyzed, and first law optimum operating parameters detailed. The system examined is hybrid fueled with fossil fuel and solar energy for the heat source. With the addition of a fossil-fuel combustor, the STIG can operate at its design point condition regardless of the solar insolation, thus avoiding part load inefficiencies that would penalize gas turbines for annual performance in a solar application [4].

2. REGENERATIVE GAS TURBINE CYCLE

Using air as the working fluid, the regenerative gas turbine cycle utilizes the waste heat from the turbine exhaust to preheat incoming air prior to combustion (Figure 1). By recovering this waste heat, the efficiency of a simple Brayton cycle can be increased significantly. Using waste heat in this manner is the only similarity between the regenerative cycle and steam injected cycle.

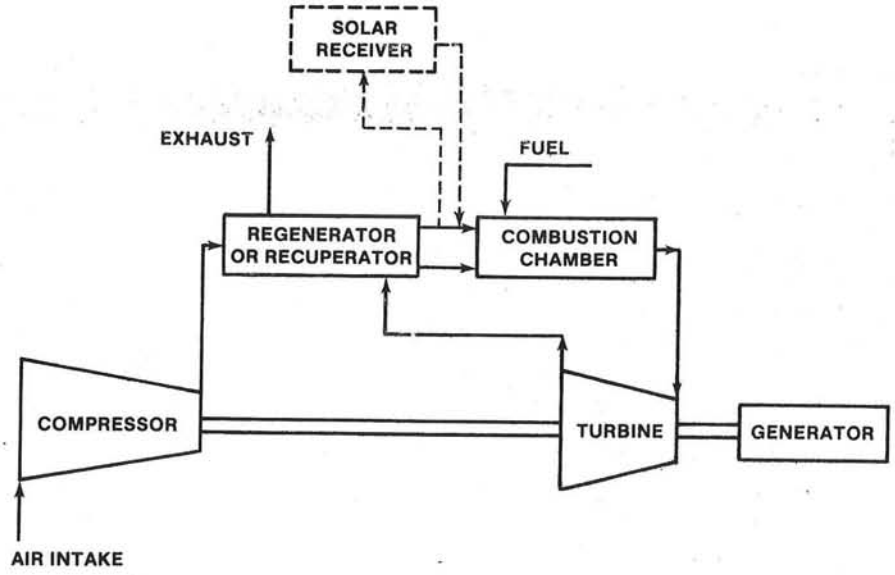

Fig. 1, Regenerative Gas Turbine Cycle

Regeneration of a simple gas turbine engine places a restriction on the engine's compression ratio because the temperature of the turbine exhaust must be larger than the discharge temperature of the compressor. The heat transfer rate will depend on the temperature difference between the two fluid streams. The effect of increasing the pressure ratio (PR) to increase the cycle efficiency is diminished because higher compression ratios mean higher turbine expansion ratios, resulting in lower turbine exhaust temperatures and a smaller temperature difference across the regenerator. Additionally, with increased PR, more work is required to compress the air.

The actual transfer of waste heat is not a simple matter for a large gas turbine power plant. Typically, the turbine exhaust location is not close to the compressor discharge. As a result, a scheme to transfer heat between the two areas is done with insulated ducts, which contribute to increased pressure drop, heat loss, and reduced system efficiency.

3. COMBINED CYCLE

A combined cycle uses the Brayton and Rankine engines but does not mix their respective working fluids like the steam injected cycle. The waste heat from the Brayton cycle is used to boil the water for the Rankine cycle. Since the fluid streams are separate, two power turbines are required instead of one (Figure 2).

The boiler of the combined cycle serves an identical function to the heat recovery steam generator (HRSG) in the STIG cycle by using waste heat from the Brayton cycle to evaporate water. However, in the case of the combined cycle the water exiting the boiler must be far enough into the superheat region so that condensation does not occur during expansion through the steam turbine. This requirement places a significant limitation on the steam boiler.

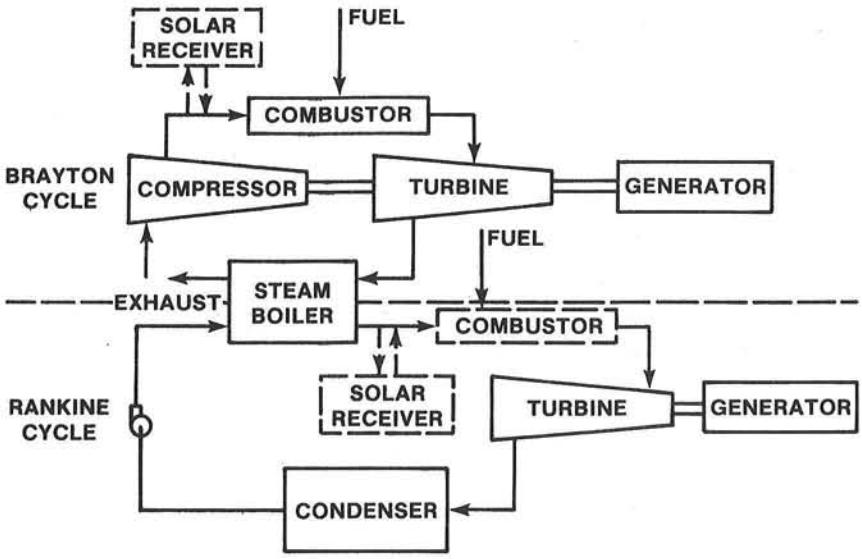

Fig. 2, Combined Cycle

The boiler must be designed large enough to superheat the water and yet not add excessive pressure drop. An alternative to this cycle would be the addition of a fossil-fuel fired boiler and/or solar augmented system to maintain a superheat state for the Rankine turbine. It will be seen that in the STIG cycle the requirement for superheated steam from the heat exchanger is unnecessary because any wet steam will be superheated in the combustor.

4. WATER INJECTED GAS TURBINE

Water injection is used to increase power output from gas turbine cycles. This method has been used for jet engines in aircraft to increase the mass flow through the turbine for additional thrust during take-off. Recently, however, water injection has been used to control air pollution in gas turbine power plants by reducing the NO_x levels.

For pollution control water is introduced into the air stream after the compressor to the point of saturation. The amount of water injected must be in correct proportion to the air mass flow so that complete vaporization of the injected water takes place prior to the regenerator. The steam-air mixture recovers the exhaust heat from the turbine exhaust before entering the combustion chamber. With this steam-air mixture the flame temperature in the combustion chamber is reduced, resulting in lower NO_x levels in the system's exhaust (Figure 3).

Although the same two working fluids are used for the water injection cycle and the STIG cycle, the operation and design of the water injection is different. As a result, there are two factors which limit the water injection cycles ability to achieve the thermal efficiency of the STIG cycle. First, the steam-air mixture used to recover heat in the regenerator has a specific heat capacity approximately a thousand times less than the water vaporization method used in the STIG cycle. As a result, less energy

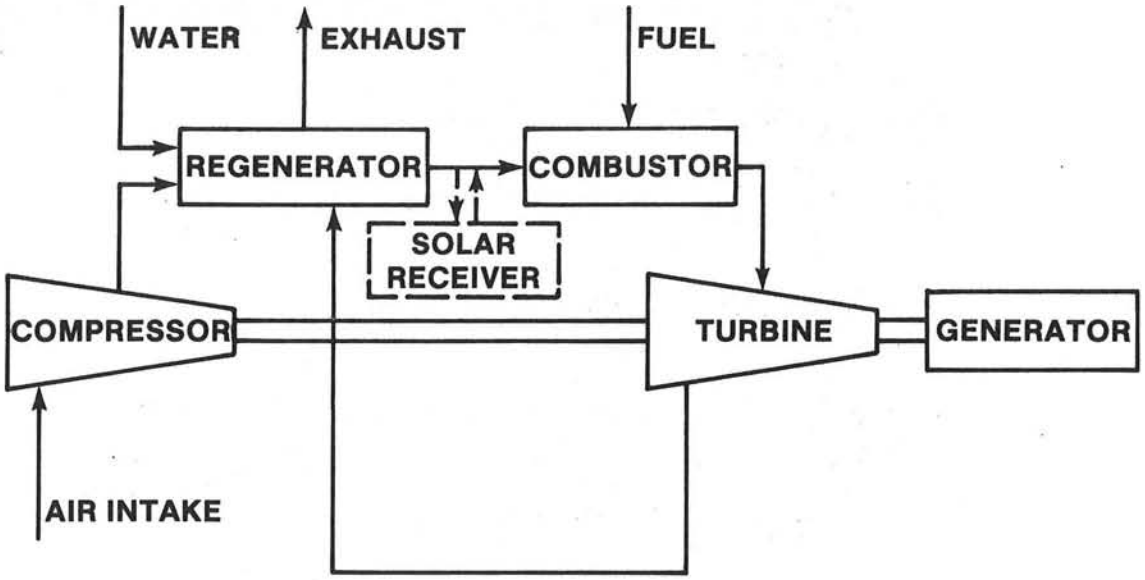

Fig. 3, Water Injected Gas Turbine

is extracted from the turbine exhaust gas. Second, the pressure ratio (PR) limitation imposed on the regenerative gas turbine also applies to the water-injected cycle. By increasing the pressure ratio (PR) to improve cycle efficiency, a smaller ΔT occurs across the regenerator, thus less heat transferred. In addition, increased work to compress the air is required.

5. STEAM INJECTED GAS TURBINE CYCLE

The STIG cycle can be thought of as two separate thermodynamic cycles that have been combined in a way to complement one another. The cycle begins with water pressurized to a level slightly higher than the exit pressure of the compressor (Figure 4). The water is heated in the heat recovery steam generator (HRSG) and injected into the solar receiver and combustion chamber where the steam is mixed with air from the compressor. From the combustion chamber the steam-air mixture is expanded through a turbine and then exhausted through the counter flow HRSG. The steam-air mixture passed through the HRSG drops to a temperature no lower than the saturation temperature of the water in the mixture. A separate condenser could be utilized to condense the water out of the steam-air mixture. A portion of the condensed liquid could be treated and returned to the feed water pump to be recirculated through the cycle. The remaining condensed liquid would be routed to a cooling tower and used for condensing further steam-air mixtures or discarded and make-up water could be added (Figure 5). Under most situations no more than 3 kg/kWh would be required for make-up [5].

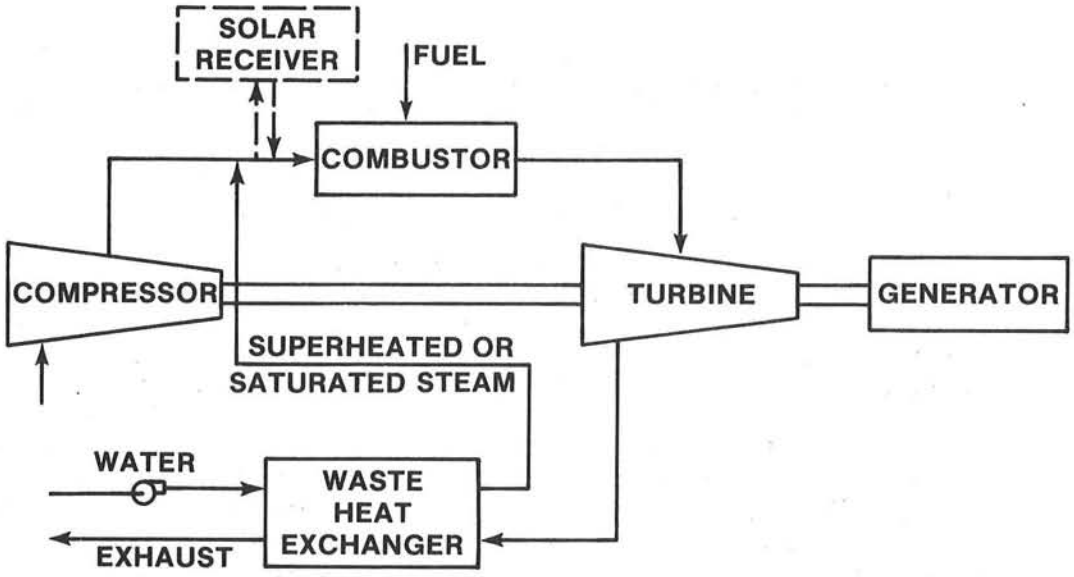

Fig. 4, Steam Injected Gas Turbine

Also, by closing the cycle, the possibility of using working fluids other than a steam-air mixture could further improve the thermal efficiency.

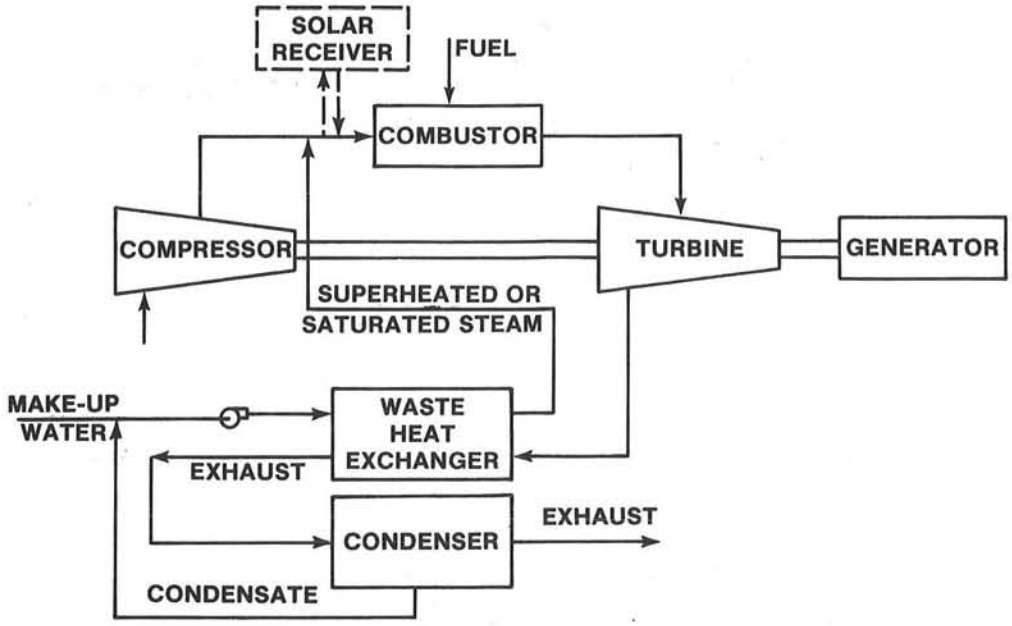

Fig. 5, Closed STIG Cycle

The fundamental advantage of the STIG cycle is that it combines the advantage of low back-work ratio (W_c/W_t) of the Rankine cycle, with the very high temperature heat addition process of the Brayton cycle. In addition,

almost complete exhaust heat regeneration can be used to further enhance cycle efficiency.

In order for the STIG cycle to maximize the thermal efficiency several operating parameters must be considered. These parameters include the turbine inlet temperature (TIT), pressure ratio (PR), pinch point temperature difference (ΔT_p) of the HRSG and the steam-air flow ratio (X).

6. ANALYSIS OF STEAM INJECTED GAS TURBINE FOR SOLAR APPLICATION

Figure 6 is an example of a STIG cycle engine with several parabolic dishes. In this configuration the solar energy system consists of several parabolic concentrators, with each concentrator reflecting the beam radiation to a solar receiver. The receiver absorbs this thermal energy and delivers it to the working fluid which is used in the STIG cycle. Gas turbines in this solar application would have the thermal energy delivered from several parabolic dishes. Power levels would be 200 kWe to 1 MWe. Previous gas turbines with power levels 5 to 10 kWe have followed the concept one engine per dish. However, at these lower power levels gas turbines are confronted with problems which are not factors with larger units. Some of these factors include component tolerances and system pressure drops [6]. For solar applications the system would be hybridized with a fossil fuel boiler to maintain operation of the system at the turbomachinery's design point, ie. turbine inlet temperature.

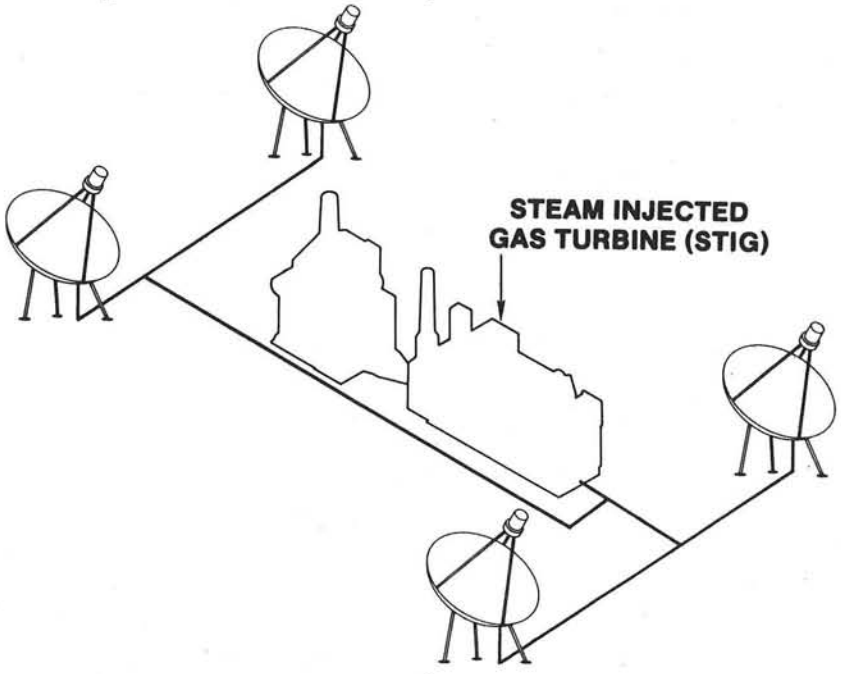

Fig. 6, Steam Injected Cycle with Parabolic Dish Concentrators

Figure 7 illustrates a central receiver system using a steam injected gas turbine engine. The engines in this application would be much larger, 1 MWe to 10 MWe, than would be possible from several parabolic dishes.

Without fixing the steam injected cycle to a particular solar system, a generic analysis can be made of the cycle. Figure 8 diagrams the basic

cycle with each component. To examine this system as a whole the individual components are analyzed and their operating parameters described mathematically.

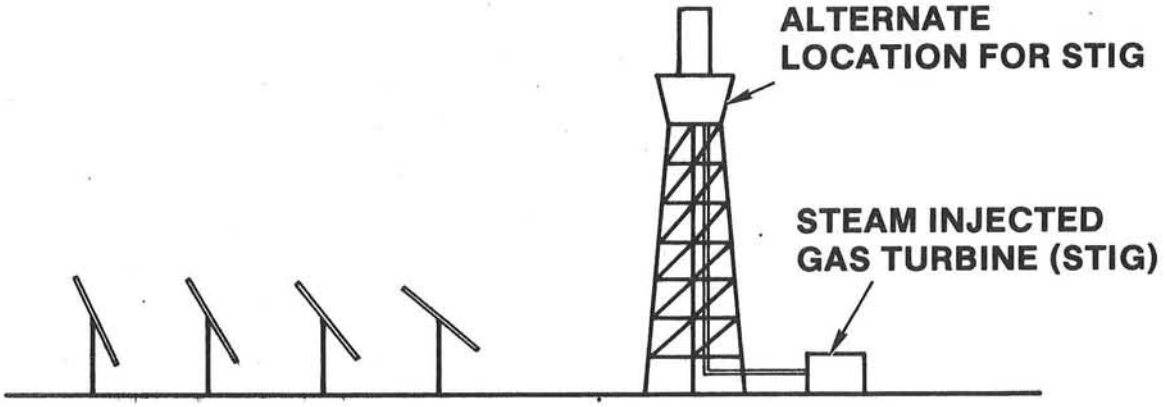

Fig. 7, Steam Injected Cycle with Central Receiver

As previously mentioned the STIG cycle is comprised of a Brayton cycle and regenerative Rankine cycle. Each cycle along with its interdependence can be illustrated on a temperature-entropy diagram in Figure 9.

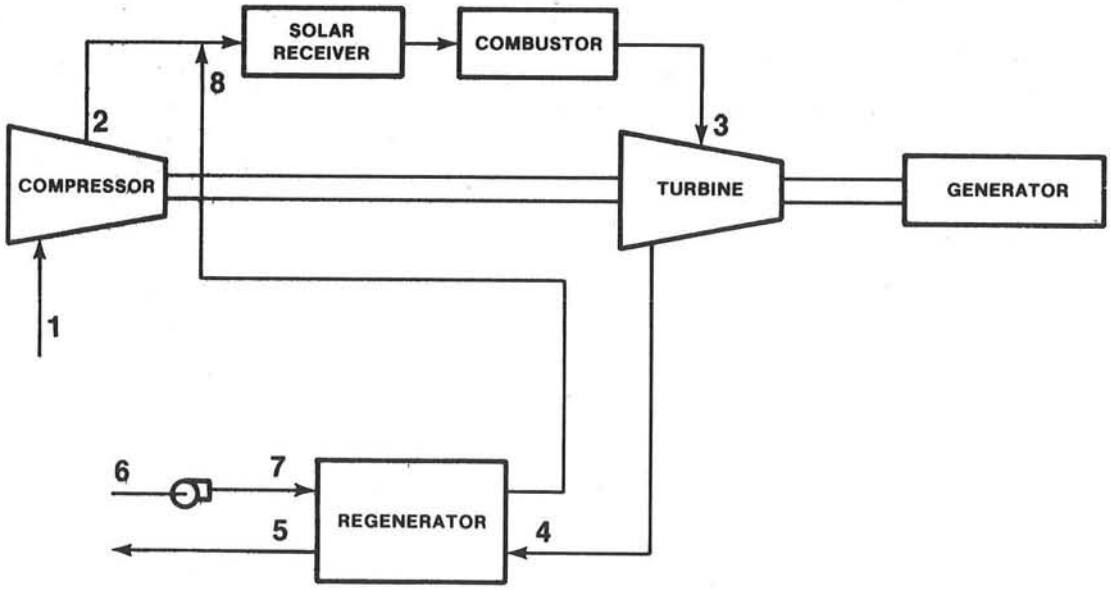

Fig. 8, STIG Cycle

The idealized Brayton cycle begins with atmospheric air at state "1" which is compressed to state "2." The addition of solar energy and fossil-fuel energy enables the cycle to reach the turbine inlet temperature (TIT) at state "3." Expansion through the turbine brings the thermodynamic state to "4" [7]. Finally with heat transfer to the Rankine fluid and some additional cooling, the thermodynamic state is returned ideally* to point "1."

(*Note: In reality this cycle is open. However, for analysis purposes, the cycle is completed.)

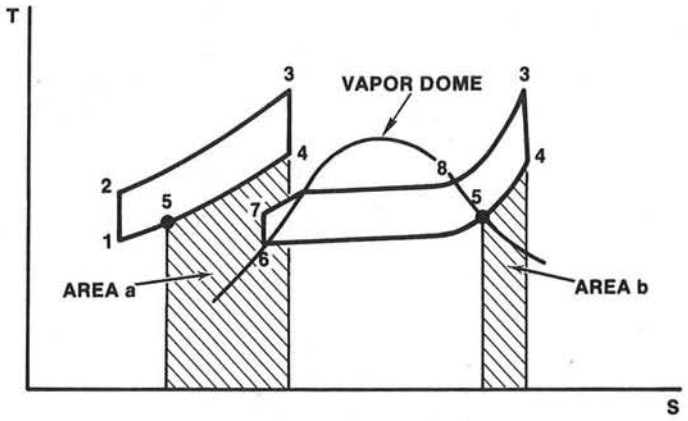

Fig. 9, Temperature - Entropy Diagram

The Rankine side of the STIG cycle begins with water at state "6," which is pumped to a pressure at state "7," which is slightly higher than the pressure at state "2." This high pressure liquid is heated through the HRSG to state "8." The temperature at "8" cannot exceed the exhaust temperature of the turbine at point "4," which is the high temperature of the HRSG. The steam is then mixed with the air and the combination is heated with solar energy and fossil fuel to reach the TIT at point "3." Expansion through the turbine brings the mixture to state "4." From state point "4" exhaust heat from the steam makes this a regenerative Rankine cycle. From state "4" the water is condensed out of the steam-air mixture and returned to state "6." Part of the waste heat from the Brayton and Rankine cycles, areas "a" and "b" respectively, are used to heat the water to steam before the two fluid streams are mixed.

The thermal efficiency, η_{th}, for this cycle is given by the following expression.

$$\eta_{th} = \frac{W_t + W_c + W_p}{Q_h} \quad . \qquad (1)$$

The parameters needed to evaluate the efficiency are the turbine work, W_t, compressor work, W_c, pump work, W_p, and the energy input, Q_h, from the high temperature heat sources.

The parameters W_t, W_c, W_p, and Q_h can be estimated by assuming isentropic changes for an ideal gas along with uniform-state, uniform-flow processes.

The compressor work, W_c, for a given air flow rate is (see Figure 8 and 9 for state points):

$$W_c = m_a c_{pa} T_1 (PR^{\phi} - 1)(1/\eta_c) \quad . \qquad (2)$$

where, PR - pressure ratio, (P_2/P_1)
ϕ - k/(k-1)
k - specific heat ratio of air
m_a - air mass flow, (kg/s)
η_c - compressor efficiency

The turbine work, W_t, for a given steam-air flow rate is:

$$W_t = mc_p\eta_t T_3[1 - (\frac{1}{\eta_{pl} PR})^{\phi}] \quad . \tag{3}$$

where, m - total mass flow, (kg/s)
η_t - turbine efficiency

A pressure loss factor, η_{pl}, has been included when determining the turbine work. This factor accounts for the pressure drops in the combustor, receiver, regenerator and ducting, which is typically, 5%-10%. In this analysis 5% was assumed.

Combining the fluid streams will change the specific heat, C_p, of the total mass flowing through the turbine. This can be accounted for using the following relationships:

$$C_p = (m_s/m_a)\, c_{ps} + c_{pa} \quad , \tag{4}$$

$$c_{pa} = 1.003 + 1.81 \times 10^{-4} T \quad , \text{ and} \tag{5}$$

$$c_{ps} = 4.6 - 103.6T^{-1/2} + \frac{967.2}{T} \quad . \tag{6}$$

T in Kelvins is an average temperature at which the process takes place [8].

The pump work, W_p, for a given water flow rate is:

$$W_p = v\,(P_7 - P_6)(1/\eta_p)\, m_s \quad , \tag{7}$$

where v is the specific volume of water. Under most conditions the pump work is an insignificant portion of the parasitic power.

To determine the heat, Q_h, required for the cycle, a control volume is drawn around the combustor and solar receiver. An energy balance is performed and Q_h is determined by:

$$Q_h = m_a c_{pa}(T_3 - T_2) + m_s c_{ps}(T_3 - T_8) \quad . \tag{8}$$

Before Q_h can be evaluated, several state point temperatures must be determined; in particular, temperatures at points 2, 3, 4, and 8.

The compressor exit temperature, T_2, is calculated assuming an ideal gas and an isentropic compressor efficiency, η_c, to give:

$$T_2 = T_1 \left(1 + \frac{PR^{\phi}}{\eta_c} - 1/\eta_c\right) . \tag{9}$$

The temperature, T_3, is the TIT. For this analysis T_3 is an independent variable. The entire system will be designed to operate for a particular TIT.

The turbine exhaust temperature, T_4, is calculated assuming an ideal gas and isentropic turbine efficiency, η_t, to obtain:

$$T_4 = T_3[1 - \eta_t + \eta_t(\frac{1}{\eta_{pl} PR})^{\phi}] . \tag{10}$$

To determine the steam temperature, T_8, exiting the HRSG an energy balance is required between the two fluid streams. For this ideal case the change in enthalpy for the steam-air mixture equals the change in enthalpy for the water-steam mixture of the HRSG. The equation for the energy balance is given by:

$$m\Delta h_{4-5} = m_s \Delta h_{7-8} . \tag{11}$$

The HRSG in this analysis is assumed to consist of an economizer, boiler and superheater. A typical temperature distribution of both flow streams through the HRSG can be seen in Figure 10 [8], [9].

The heat released from the turbine exhaust to the water-steam side of the HRSG is given by:

$$Q_{4-5} = Q_{4-p} + Q_{p-5} , \tag{12}$$

$$Q_{4-p} = mc_p(T_4 - T_{sat} - \Delta T_p) , \text{ and} \tag{13}$$

$$Q_{p-5} = mc_p(T_{sat} + \Delta T_p - T_5) . \tag{14}$$

where, ΔT_p, the pinch point temperature, is defined as the minimum temperature difference between the steam-air side and the water-steam side of the HRSG.

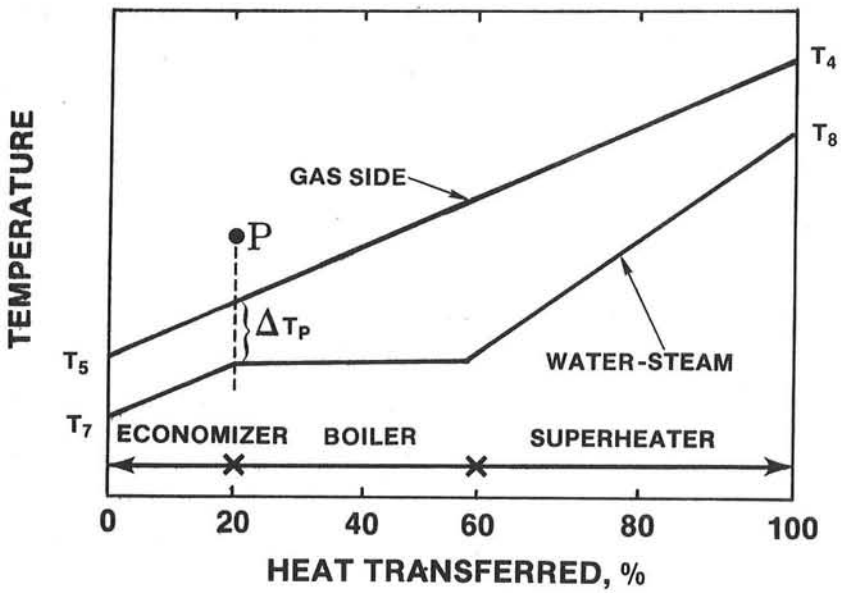

Fig. 10, Temperature Distribution in HRSG

The pinch pint has a direct effect on the HRSG's surface area. The surface area in turn determines the amount of heat transferred, maximum steam flow and the cost of the HRSG. Typically ΔT_p is designed to be 10-30°C. For this analysis ΔT_p is assumed to be 15°C [10].

In practice approximately 2% of the available exhaust energy is lost through the HRSG housing by radiation or other means.

Therefore, the heat absorbed by the water-steam is

$$Q_{7-8} = .98\ Q_{4-5} \ . \tag{15}$$

An energy balance of the HRSG results in the following equation.

$$m_w h_7 + Q_{7-8} = m_s h_8 + (m_w - m_s) h_{sat} \ . \tag{16}$$

where h_7 is the change in enthalpy of the water entering the economizer, h_{sat} is the enthalpy of the saturated water in the boiler, h_8 is the enthalpy of the steam exiting the superheater and $(m_w - m_s)$ accounts for continuous blowdown of water (usually 2% - 5% of the steam flow) to control the amount of solids in the water and prevent mineral build-up in the HRSG.

Rearranging Equation (16), the enthalpy of the exiting steam can be determined by:

$$h_8 = \frac{m_w h_7 + .98 Q_{4-5} - (m_w - m_s) h_{sat}}{m_s} \ . \tag{17}$$

Knowing the steam pressure P_7 and the steam enthalpy h_8, from Equation (17), the exit steam temperature T_8 can be determined from steam tables. The thermal efficiency of the STIG cycle can now be determined for various steam-air ratios and TITs.

7. SOLAR RECEIVER ANALYSIS

When combining a STIG cycle and solar energy, the effects of a solar receiver and concentrator, ie. collection efficiency must be considered. For this analyses only distributed receiver system will be considered. However, the differences between central and distributed systems will be noted in the appropriate equations. Figure 11 gives the details of the receiver and parabolic concentrator assumptions used for this analysis.

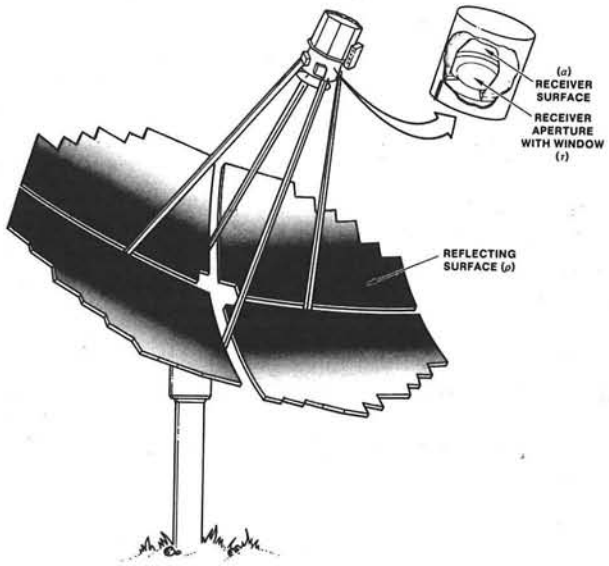

Fig. 11, Cavity Receiver/Parabolic Concentrator

Based on an energy balance for the receiver and characteristics of the concentrator a definition for the collection efficiency, η_{col} of solar energy system can be determined as follows [11].

$$\eta_{col} = \frac{\dot{Q}_{net}}{I_o A_c} \quad . \tag{18}$$

$\dot{Q}_{net}$ - net thermal energy out of receiver, (W)
I_o - direct normal solar insolation, (W/m^2)
A_c - aperture area of collector, (m^2)

The net thermal energy, $\dot{Q}_{net}$ collected by the receiver is given by:

$$\dot{Q}_{net} = \dot{Q}_{in} - \dot{Q}_{loss} \quad . \tag{19}$$

where, $\dot{Q}_{in}$ - thermal energy absorbed by receiver, (W)
$\dot{Q}_{loss}$ - thermal energy lost from receiver, (W)

The thermal energy into the receiver is defined as:

$$\dot{Q}_{in} = I_o A_c \rho \tau \alpha (n)(\eta_f) \quad . \tag{20}$$

where, ρ - specular reflectance of concentrator surface
τ - transmittance of window in receiver aperture
α - absorptance of receiver surface
n - total number of heliostats for a central receiver, only
η_f - efficiency of heliostats field includes: cosine loss, shadowing, blocking, atmosphere attenuation for a central receiver, only

The terms ρ, τ, and α are characteristics of the concentrator and solar receiver. In most situations they can be considered a constant and labeled as one term called the optical efficiency η_{opt}. Equation (20) then becomes:

$$\dot{Q}_{in} = I_o A_c \eta_{opt} \quad . \tag{21}$$

The thermal energy lost from the receiver is comprised mainly of convection heat transfer and radiation heat transfer through the aperture of the receiver [12].

$$\dot{Q}_{loss} = A_r h(T_{rs} - T_a) + \sigma A_r \epsilon F(T_{rs}^4 - T_a^4) \quad . \tag{22}$$

where, A_r - aperture area of receiver, (m^2)
h - convection heat transfer coefficient, (W/m^2 °C)
T_{rs} - surface temperature of receiver absorber, (°K)
T_a - ambient air temperature, (°K)
σ - Stefan-Boltzmann Constant, (5.67×10^{-8} W/m^2 °K)
ϵ - effective emissivity of receiver aperture
F - radiation shape factor

The convection heat transfer is influenced by the receiver attitude during operation as well as its design. For example, a STIG system using a cavity type design would probably use a window over the receiver aperture. This window would reduce the convection losses, but would have an associated transmission loss through the window that would result in a reduced optical efficiency, η_{opt}. For a windowless receiver it has been shown that the maximum heat loss will occur with the receiver aperture pointing 60° above a

horizontal position [13]. In most operating situations for a distributed receiver system, however, the receiver aperture will be oriented downward reducing the heat loss substantially.

The temperature of the absorber surface and the radiation shape factor are of concern in radiation heat transfer from the solar receiver. As the operating temperature of the receiver increases the heat loss by T^4.

By substitution and reduction, Equation (18) can be transformed into the following equation which is concentrator and receiver specific.

$$\eta_{col} = 1 - \frac{h(T_{rs} - T_a) - \sigma \epsilon F(T_{rs}^4 - T_a^4)}{CR\ I_o\ \eta_{opt}} \quad . \tag{23}$$

where, $CR = A_c/A_r$, concentration ratio

$U \approx 5$, windowed cavity receiver, $W/m^2 {}^\circ C$

$T_{rs} = 600 - 1200\ ^\circ C$

$T_a = 20\ ^\circ C$

$CR = 1500$

$I_o = 50 - 1000\ W/m^2$

$\sigma = 5.667 \times 10^{-8}\ W/m^2\ K^4$

$e = .95$

$F = 1$

$\eta_{opt} = .77$

Table 1. Receiver - Concentrator Parameters

Based on the assumption from Table (1) and Equation (23) Figure 12 indicates the predicted thermal performance of a solar cavity receiver and parabolic concentrator for various levels of insolation and operating temperatures. The actual collection performance will depend on the specific receiver designs, however, the general trend will remain the same. It is apparent from these predictions, that the operating temperature of the receiver is an important factor in the efficiency of the system. As the temperature of the receiver increases, the solar collection efficiency decreases. This reduction is largely due to radiation heat loss from the receiver.

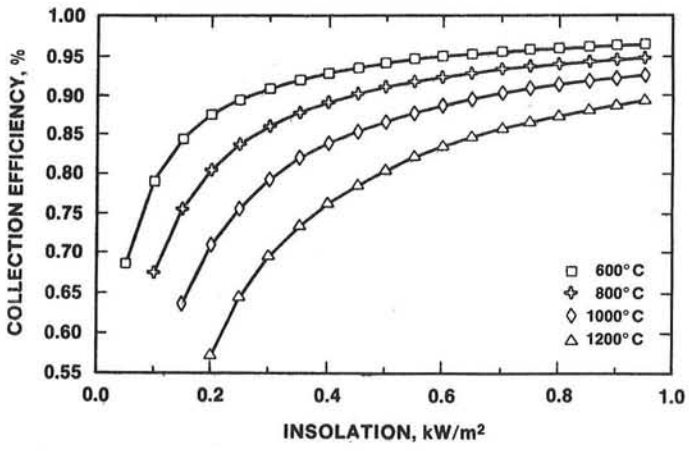

Fig. 12. Receiver Efficiency vs Insolation and T_{rs}

8. Results

To analyze the STIG cycle, a sensitivity analysis was conducted based on the variation of PR, TIT, and X. Several assumptions, however, were made for the component efficiences, state point temperatures, pressure ratios and steam flows. Table 2 summarizes the parameters specified for this analysis.

Compressor, adiabatic efficiency	$\eta_c = .83$
Turbine, adiabatic efficiency	$\eta_t = .90$
Pump	$\eta_p = .70$
Combustor	$\eta_{con} = .99$
HRSG, pinch point	$T_p = 15°C$
HRSG, exhaust temperature	$T_5 = 150°C$
PR, pressure ratio	7.5 - 15.0
TIT, turbine inlet temperature	600°C - 1200°C
X, steam - air ratio	.025 - .4

Table 2, Cycle Parameters

Figure 13 presents a three-dimensional view of the cycle efficiency, given in Equation (1), as a function of TIT and X for a PR of 12.5.

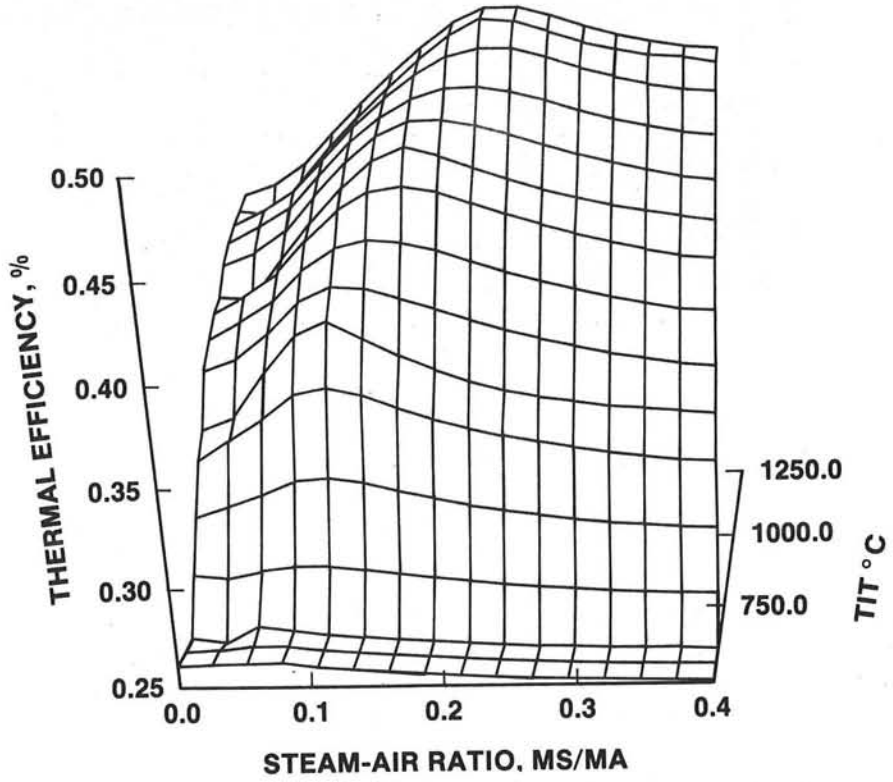

Fig. 13. 3-D Surface at Constant PR

Figure 14 presents a similar surface with the TIT of 1000°C.

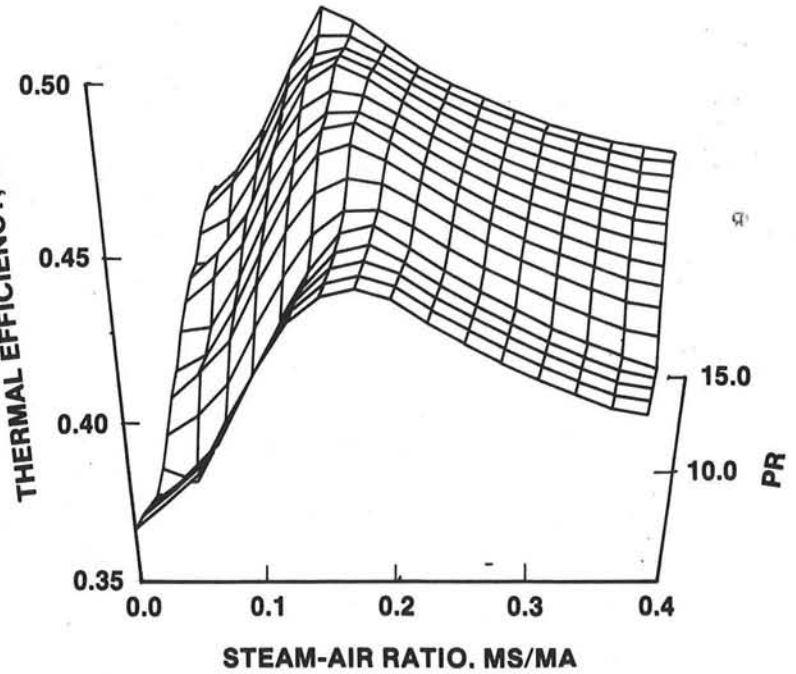

Fig. 14. 3-D Surface at Constant TIT

It is apparent that for any given PR and TIT there is a unique X, which maximizes the cycle efficiency. This results in ridges along the surfaces in Figures 13 and 14.

Figure 15 presents the STIG cycle for a TIT of 1000°C and a range of pressure ratios. This figure is a X-Y plane view of several slices through the three-dimensional surface of Figure 14.

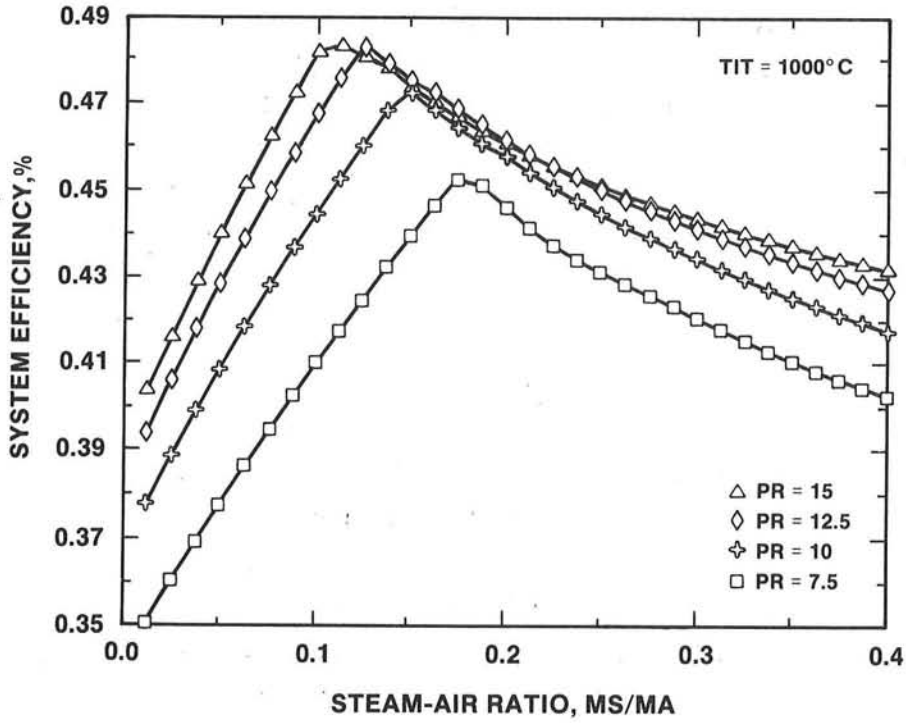

Fig. 15, STIG Cycle Efficiency vs X

The unique steam-air ratio, X_{peak}, which maximizes the cycle efficiency, is a function of the available energy in the turbine exhaust and the designed pinch point temperature T_p of the HRSG.

Figure 16 shows the properties of the steam at the exit of the HRSG for various TITs. For steam-air ratios up to X_{peak} the energy required to vaporize the water is available from the turbine exhaust. The steam, in fact, is superheated and, therefore, additional energy from a solar receiver and/or combustor is only required to heat the steam to the TIT. At X_{peak} the steam-air ratio and turbine exhaust are such that the maximum energy available from the turbine exhaust has been used to superheat the steam, resulting in the highest thermal efficiency. Beyond X_{peak} the increase in mass flow through the turbine is not sufficient to offset the additional energy required to raise the steam temperature to the TIT, causing decreased thermal efficiency.

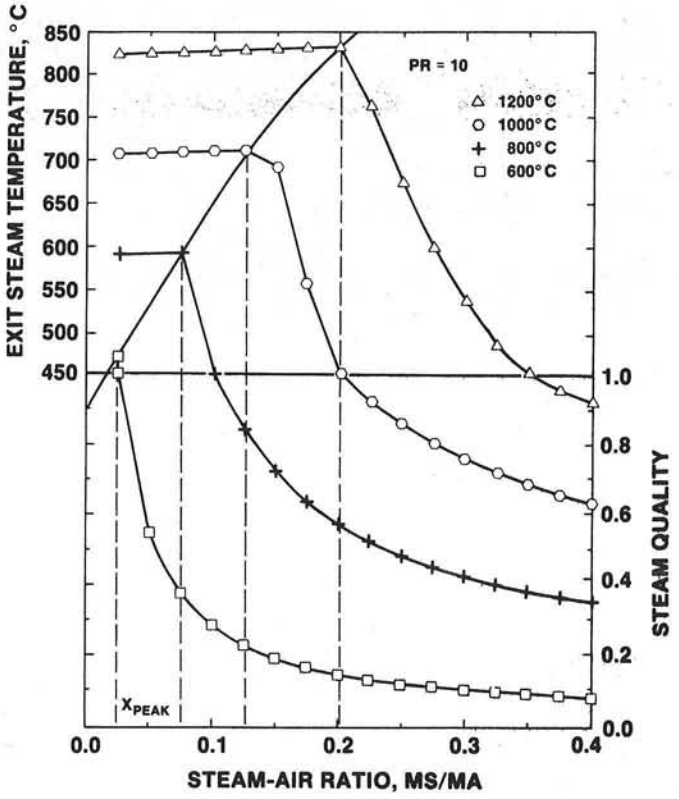

Fig. 16, Temperature/Quality/η vs X

Figure 17 is an example of the actual T_p in the HRSG as compared to the design T_p. The actual T directly relates to the steam exit temperature of the HRSG.

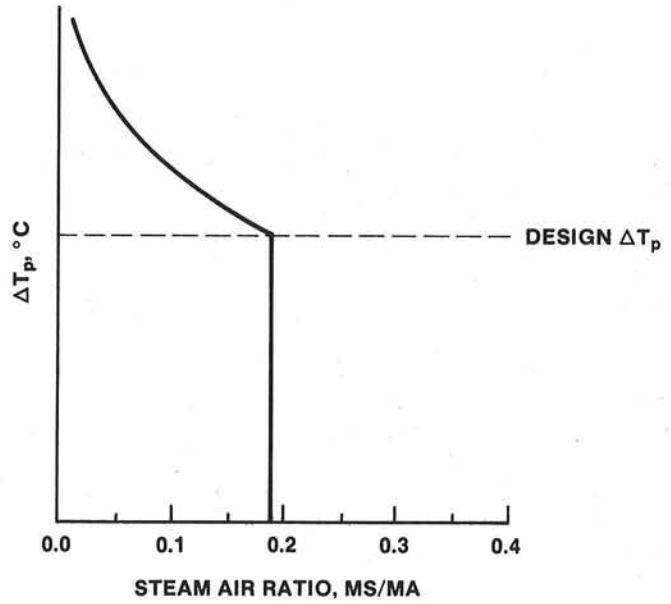

Fig. 17, Actual T_p vs Design T_p

For low steam-air ratios the actual pinch point temperature should be greater than the design T_p. This implies the lack of heat recovery from the turbine exhaust. With increased steam-air ratios the actual T_p approaches the design T_p until X_{peak} is achieved. At X_{peak} the actual T_p equals the designed T_p and the maximum heat recovery has occurred. Beyond X_{peak} the designed T_p constrains the actual T_p. As a result insufficient energy from the turbine exhaust can be recovered, and the steam temperature and quality drop.

9. CONCLUSIONS

The first-law analysis described in this paper indicates that within a defined operating region, the steam injected gas turbine (STIG) is a viable power generating cycle for solar applications. With steam injection rates of 10%-20% the STIG cycle can achieve efficiencies of 42%-48%, at TITs of 800°C and above, which can be up to 40% improvement over a simple gas turbine cycle [14].

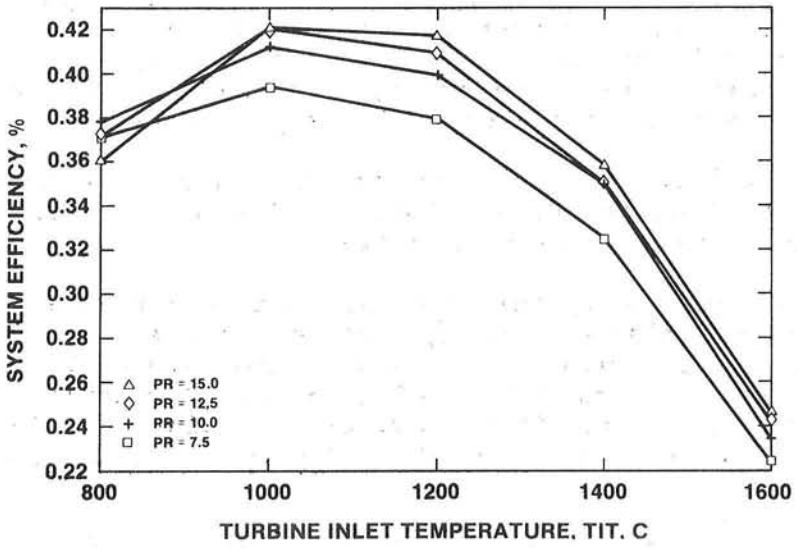

Fig. 18, Solar System Efficiency vs TIT and PR

Figure 18 indicates the optimum thermal efficiency which could be expected from a combined STIG and solar system operating at a solar insolation of 950 kW/m^2. As observed in the two previous sections, the thermal efficiency of the STIG cycle increases with operating temperature while the solar system efficiency decreases with operating temperature (Figures 12 and 15). When operating at the X_{peak} ratio this system can be expected to be 39-42% for TITs of 800°C and above. These efficiencies are based on operating the STIG cycle without additional heat input from a fossil fuel combustor. Actual system efficiencies will be slightly less due to the unaccounted heat loss in piping, etc.

Conceptually the incorporation of a solar receiver into a STIG cycle is straight-forward. The receiver placement prior to and in series with the fossil-fuel combustor would not degrade the performance of the STIG itself. With the receiver in this location the radiation heat loss through the

aperture would be minimized for all operating scenarios, ie. fossil-fuel only, solar only or a hybrid combination of the two.

To consider a combined steam injected gas turbine (STIG) and solar thermal system, several issues must be addressed. Some of these are as follows:

1. The availability of water and water treatment must be considered. Many good solar sites are located in arid regions where water is scarce.

2. Operating strategies must be considered when using solar and fossil energy to optimize the system efficiency and minimize operating costs.

3. With high pressure ratios, 7.5 - 15, and high temperatures, 800°C - 1400°C, of the STIG cycle, solar receiver design becomes a concern. The cost-effectiveness of materials to meet these operating conditions could limit this cycle for solar applications [15].

4. The specific receiver design for a solar thermal application must be verified. Various concepts of cavity receiver designs exist but few have been built and tested. However, many components, i.e. windows, ceramic matrix heat exchangers, insulation and software design codes, which are part of a total receiver design have been developed.

5. The availability, maturity, and operation of steam injected gas turbines (STIG) are limited but growing. As the STIG cycle establishes a technology base, its use will increase.

The steam injected gas turbine offers inherent advantages for medium size (500 kWe - 5 MWe) solar thermal application. Analysis has shown that within a defined operating region this cycle can offer high efficiency for a solar thermal system. In addition, smaller concentrator sizes for a given power output could be expected. Compared to other cycles, the STIG cycle could have lower capital costs, reduced complexity, and a compact modular system design.

Because the basic technology for the STIG cycle and receiver design is available further research and development would be a minimum. This could make a solar augmented STIG cycle an excellent mid-term and long-term candidate for parabolic dish and central receiver solar applications.

REFERENCES

1. D. G. Wilson, The Design of High-Efficiency Turbomachinery and Gas Turbines (Boston: The MIT Press, 1984), p. 24.

2. Sanders Associates, Inc., Parabolic Dish Module Experiment Final Test Report, SAND85-7007 (Albuquerque: Sandia National Laboratories, March 1986), pp.44-74.

3. D. Y. Cheng, Parallel-Compound Dual-Fluid Heat Engine, International Power Technology, Patent 3,978,661, September 7, 1976.

4. L. L. Lukens, Dish Electric Systems Heat Engine Assessment. SAND85-0522 (Albuquerque: Sandia National Laboratories, June 1985).

5. B. G. Ediss, "The Steam Injection Gas Turbine Cycle," Process Technology International, Vol. 17, No. 11, November 1972, pp. 864-866.

6. K. L. Linker, Heat Engine Development for Solar Thermal Dish-Electric Power Plants, SAND86-0289 (Albuquerque: Sandia National Laboratories, September 1986).

7. P. J. Potter, Power Plant Theory and Design (New York: John Wiley & Sons), pp. 556-571.

8. E. D. Larson and R. H. Williams, "Technical and Economic Analysis of Steam-Injected Gas-Turbine Cogeneration," Energy Sources: Conservation and Renewables, (New York:American Institute of Physics, 1985).

9. W. E. Fraize and C. Kinney, "Effects of Steam Injection on the Performance of Gas Turbine Power Cycles," Journal of Engineering for Power, April 1979, pp. 217-227.

10. V. L. Eriksen, J. M. Froemming and M. R. Carroll, "Design of Gas Turbine Exhaust Heat Recovery Boiler Systems," ASME Paper 84-GT-126.

11. W. B. Stine and R. W. Harrigan, Solar Energy Fundamentals and Design, (New York: John Wiley & Sons), pp. 119-121

12. W. B. Stine and R. W. Harrigan, Solar Energy Fundamentals and Design, (New York: John Wiley & Sons), p. 196

13. W. B. Stine and C. G. McDonald, "Cavity Receiver Heat Loss Measurements," Paper Presented at ASME Solar Energy Division Conference, April 1988

14. White Paper from Mechnical Technology Inc. to Sandia National Laboratories.

15. R. J. Copeland, "High Temperature Applications Study, "Proceedings of the Department of Energy Solar Central Receiver Technology Annual Meeting," SAND85-8241 (Livermore: Sandia National Laboratories, December 1985), pp. 393-403.

Appendix A

NOMENCLATURE

c_p	total constant pressure specific heat, (KJ/kg-K)
c_{pa}	constant pressure specific heat of air, (KJ/kg-K)
c_{ps}	constant pressure specific heat of steam, (KJ/kg-K)
h_l	enthalpy of liquid, (KJ/kg)
h_{fg}	latent heat of vaporization, (KJ/kg)
h_s	superheat enthalpy, (KJ/kg)
I_o	direct normal insolation, (W/m^2)
m	total mass flow, (kg/s)
m_a	mass flow of air, (kg/s)
m_s	mass flow of steam, (kg/s)
m_w	mass flow of water, (kg/s)
PR	compressor pressure ratio
TIT	turbine inlet temperature
T_s	sensible temperature, (°C or °K)
T_{sat}	saturation temperature, (°C or °K)
T_{rs}	temperature of receiver surface
T_a	temperature of ambient
X	steam-air ratio (m_s/m_a)
X_{peak}	optimum steam-air ratio

DISTRIBUTION:

AAI Corporation
P.O. Box 6787
Baltimore, MD 21204

Acurex Aerotherm
555 Clyde Avenue
Mountain View, CA 94039
Attn: H. Morse

Alabama A&M University (2)
Department of Physics
P.O. Box 271
Normal, AL 35762
Attn: M. D. Aggarwal
A. Tan

Alpha Solarco
600 Vine St.
Cincinnati, OH 45202

Applied Concepts
405 Stoney Creek Blvd.
P.O. Box 490
Edinburg, VA 22824
Attn: J. S. Hauger

Applied Concepts
2501 S. Larimer County Rd. 21
Berthound, CO 80513
Attn: S. Pond

Arizona Public Service Co. (2)
P.O. Box 21666
Phoenix, AZ 85036
Attn: J. McGuirk
E. Weber

Australian National University
Department of Engineering Physics
P.O. Box 4
Canberra ACT 2600, AUSTRALIA
Attn: Prof. Stephen Kaneff

B&E Technical Services Inc.
Attn: William R. Lang
6314 S. Piccadilly St.
Aurora, CO 80016

Barber-Nichols Engineering
6325 West 55th Ave.
Arvada, CO 80002
Attn: R. Barber

BDM Corporation
1801 Randolph Street
Albuquerque, NM 87106
Attn: W. E. Schwinkendorf

Battelle Memorial Institute
Pacific Northwest Laboratory
4000 NE 41st St.
Seattle, WA 98105
Attn: K. Drumheller

Battelle Memorial Institute
Pacific Northwest Laboratory
P.O. Box 999
Richland, WA 99352
Attn: T. Williams

Bechtel Group, Inc.
P.O. Box 3965
50 Beale Street
San Francisco, CA 94119
Attn: P. DeLaquil

Black & Veatch
P.O. Box 8405
Kansas City, MO 64114
Attn: J. C. Grosskreutz

Boeing Engineering & Construction
P.O. Box 3999
Seattle, WA 98124
Attn: R. Gillette

Budd Company (The)
Fort Washington, PA 19034
Attn: W. W. Dickhart

Budd Company (The)
Plastic R&D Center
356 Executive Drive
Troy, MI 48084
Attn: K. A. Iseler

Burns & Roe (2)
800 Kinderkamack Road
Oradell, NJ 07649
Attn: G. Fontana
R. Cherdack

California Energy Commission
1516 - 9th Street
Sacramento, CA 95814
Attn: Alec Jenkins

Cal Poly State University
San Luis Obispo, CA 93407
Attn: E. J. Carnegie

California Institute of Technology
Aeronautics Library
MS 205-45
Pasadena, CA 91125
Attn: Jean Anderson

California Polytechnic University
Dept. of Mechanical Engineering
Pomona, CA 91768
Attn: W. B. Stine

Chicago Bridge and Iron
800 Jorie Blvd.
Oak Brook, IL 60521
Attn: J. M. Shah

Colorado State University
Ft. Collins, CO 80523
Attn: T. G. Lenz

Columbia Gas System Service Corp.
1600 Dublin Road
Columbus, OH 43215
Attn: J. Philip Dechow

Datron Systems, Inc.
200 West Los Angeles Ave.
Simi Valley, CA 93065-1650

DFVLR (2)
Institute for Technical Thermodynamics
Attn: W. Schiel
R. Kohne
Pfaffenwaldring 38-40
7000 Stuttgart 80
FEDERAL REPUBLIC OF GERMANY

DSET
Box 1850
Black Canyon Stage I
Phoenix, AZ 85029
Attn: G. A. Zerlaut

Donnelly Corporation
49 West Third Street
Holland, MI 49423
Attn: M. DeVries

Electric Power Research Inst. (2)
3412 Hillview Avenue
Palo Alto, CA 94303
Attn: E. A. Demeo
J. E. Cummings

Energy Technology Engr. Ctr.
Rockwell International Corp.
P.O. Box 1449
Canoga Park, CA 91304
Attn: W. L. Bigelow

ENTECH, Inc. (3)
P.O. Box 612246
DFW Airport, TX 75261
Attn: R. R. Walters
W. Hesse
M. O'Neill

Eurodrive, Inc.
30599 San Antonio Rd.
Hayward, CA 94544

Florida Solar Energy Center
300 State Road 401
Cape Canaveral, FL 32920
Attn: Library

Ford Motor Company
Glass Div., Technical Center
25500 West Outer Drive
Lincoln Park, MI 48246
Attn: V. L. Lindberg

Foster Wheeler Solar Dev. Corp. (2)
12 Peach Tree Hill Road
Livingston, NJ 07039
Attn: M. D. Garber
R. J. Zoschak

Garrett Turbine Engine Co.
111 South 34th Street
P.O. Box 5217
Phoenix, AZ 85010
Attn: Ed Strain

Georgia Power Co. (2)
7 Solar Circle
Shenandoah, GA 30264
Attn: E. Ney
E. Ellingston

Heery Energy Consultants, Inc.
Project Energy Manager
880 West Peachtree St. NW
Atlanta, GA 30309
Attn: Glenn Bellamy

Highland Plating
10001 N. Orange Drive
Los Angeles, CA 90038
Attn: M. Faith

Industrial Solar Technologies
5775 West 52nd Ave.
Denver, CO 80212
Attn: Randy Gee

Institute of Gas Technology
Attn: Library
34245 State Street
Chicago, IL 60616

Jet Propulsion Laboratory
4800 Oak Grove Drive
Pasadena, CA 91109
Attn: M. Alper

Kearney & Associates
14022 Condessa Drive
Del Mar, CA 92014
Attn: David W. Kearney

LaCour Kiln Service
P.O. Box 247
Canton, MS 39046
Attn: J. A. LaCour

LaJet Energy Co. (2)
P.O. Box 3599
Abilene, TX 79604
Attn: Monte McGlaun
Carl Williams

L'Garde Inc.
15181 Woodlawn Ave.
Tustin, CA 92680-6419
Attn: Mitchell Thomas

John Lucas
865 Canterbury Road
San Marino, CA 91108

Luz International Limited
924 Westwood Blvd.
Los Angeles, CA 90024
Attn: Dr. D. W. Kearney

Martin Marietta Corp. (2)
12250 So. Hwy. 75
Littleton, CO 80125
Attn: Tom Tracey
H. Wroten

McCarter Corporation
200 E. Washington St.
P.O. Box 351
Norristown, PA 19404
Attn: R. A. Powell

McDonnell-Douglas Astronautics
Company (3)
5301 Bolsa Avenue
Huntington Beach, CA 92647
Attn: R. L. Gervais
J. Rogan
D. Steinmeyer

Mechanical Technology, Inc. (2)
968 Albany Shaker Road
Latham, NY 12110
Attn: G. R. Dochat
J. Wagner

Meridian Corporation
4300 King St.
Suite 400
Alexandria, VA 22302-1508
Attn: D. Kumar

Midwest Research Institute (2)
425 Volker Blvd.
Kansas City, MO 64110
Attn: R. L. Martin
J. Williamson

NASA Lewis Research Center
21000 Brook Park Road
Cleveland, OH 44135
Attn: R. Beremand, MS 301-2
J. Savino, MS 301-5
T. McCoy, MS 301-5
R. Puthoff
R. Corrigan

New Mexico Solar Energy Institute
New Mexico State University
Box 3SOL
Las Cruces, NM 88003

Parsons of California
P.O. Box 6189
Stockton, CA 95206
Attn: D. R. Biddle

PG&E
3400 Crow Canyon Rd.
San Ramon, CA 94583
Attn: J. Iannucci
G. Braun

Power Kinetics, Inc.
415 River Street
Troy, NY 12180-2822
Attn: W. E. Rogers

Renewable Energy Institute
1001 Connecticut Avenue NW
Suite 719
Washington, DC 20036
Attn: Kevin Porter

Research Systems, Inc.
Suburban Trust Bldg.,
Suite 203
5410 Indian Head Hwy.
Oxon Hill, MD 20745
Attn: T. A. Chubb

Rockwell International
Energy Systems Group
8900 De Soto Avenue
Canoga Park, CA 91304
Attn: T. Springer

Rockwell International
Space Station Systems Division
12214 Lakewood Blvd.
Downey, CA 90241
Attn: I. M. Chen

Sanders Associates
144 D.W. Highway South
C.S. 2034
Nashua, NH 03061-2034
Attn: J. Kesseli

Science Applications
International Corp.
10401 Roselle Street
San Diego, CA 92121
Attn: Barry Butler

Solactor Corporation
2065 Keystone Blvd.
Miami, FL 33181
Attn: Joseph Womack

Solar Energy Industries Association (2)
Suite 610
1730 North Lynn St.
Arlington, VA 22209-2009
Attn: C. LaPorta
S. Sklar

Solar Energy Research Inst. (4)
1617 Cole Blvd.
Golden, CO 80401
Attn: B. P. Gupta
J. Thornton
M. Murphy
D. Hawkins

Solar Kinetics, Inc.
P.O. Box 540636
Dallas, TX 75354-0636
Attn: J. A. Hutchison

Solar Steam
P.O. Box 32
Fox Island, WA 98333
Attn: D. E. Wood

Southern California Edison (3)
P.O. Box 800
Rosemead, CA 92807
Attn: J. N. Reeves
P. Skvarna

SLEMCO
19655 Redberry Dr.
Los Gatos, CA 95030
Attn: A. J. Slemmons

Stearns-Catalytic Corp.
Box 5888
Denver, CO 80217
Attn: T. E. Olson

Stirling Thermal Motors
2841 Boardwalk
Ann Arbor, MI 48104
Attn: Ben Ziph

Sun Exploration and Production Co.
P.O. Box 2880
Dallas, TX 75221-2880
Attn: R. I. Benner

Sun Power, Inc.
6 Byard St.
Athens, OH 45701
Attn: Mac Thayer

Sundstrand ATG
P.O. Box 7002
Rockford, IL 61125
Attn: D. Chaudoir

Suntec Systems, Inc. (2)
Suite B-4
Loring Park Office Bldg.
430 Oak Grove St.
Minneapolis, MN 55403
Attn: Harrison Randolph
J. H. Davison

Swedlow, Inc.
12122 Western Avenue
Garden Grove, CA 92645
Attn: E. Nixon

3M-Energy Control Products (2)
207-1W 3M Center
St. Paul, MN 55144
Attn: B. Benson
J. L. Roche

Texas Tech University
Dept. of Electrical Engineering
P.O. Box 4439
Lubbock, TX 79409
Attn: E. A. O'Hair

TRW (3)
Space & Technology Group
One Space Park
Redondo Beach, CA 90278
Attn: G. M. Reppucci
A. D. Schoenfeld
J. S. Archer

U.S. Department of Energy (3)
Albuquerque Operations Office
P.O. Box 5400
Albuquerque, NM 87185
Attn: C. Garcia
D. Graves
N. Lackey

U.S. Department of Energy
Office of Solar Heat Technologies
Forrestal Building
Washington, DC 20585
Attn: Fred Morse

U.S. Department of Energy
Office of Solar Heat Technologies
Forrestal Building
Washington, DC 20585
Attn: C. Carwile

U.S. Department of Energy
Division of Solar Thermal Tech.
Forrestal Building
Washington, DC 20585
Attn: Howard S. Coleman
R. Shivers
S. Gronich
M. Scheve
F. Wilkins

U.S. Department of Energy
San Francisco Operations Ofc.
1333 Broadway
Oakland, CA 94612
Attn: R. W. Hughey

U.S. Robotics
8100 N. McCormack Blvd.
Skokie, IL 60076
Attn: Paul Collard

University of Houston (2)
Energy Laboratory; SPA
Houston, TX 77004
Attn: Lorin Vant-Hull
A. F. Hildebrandt

University of New Mexico (2)
Department of Mechanical Engr.
Albuquerque, NM 87131
Attn: M. W. Wilden
W. A. Gross

Viking Solar Systems, Inc.
1850 Earlmont Ave.
La Canada, CA 91011
Attn: George Goranson

WG Associates
6607 Stonebrook Circle
Dallas, TX 75240
Attn: Vern Goldberg

0400 R. P. Stromberg
1510 J. W. Nunziato
1513 D. W. Larson
1820 R. E. Whan
1824 J. N. Sweet
1840 R. J. Eagan
1841 R. B. Diegle
1842 R. E. Loehman
1846 D. H. Doughty
2520 N. J. Magnani
2525 R. P. Clark
2540 G. N. Beeler
2541 J. P. Abbin
3141 S. A. Landenberger (5)
3151 W. L. Garner (3)
3154 C. H. Dalin (8) for DOE/OSTI
3160 J. E. Mitchell
6000 D. L. Hartley
6200 V. L. Dugan
6220 D. G. Schueler
6221 E. C. Boes
6222 J. V. Otts
6223 G. J. Jones
6224 D. E. Arvizu
6225 H. M. Dodd
6226 J. T. Holmes
6227 K. L. Linker (10)
6227 J. A. Leonard (20)
6250 B. W. Marshall
6254 B. Granoff
7470 J. L. Ledman
7471 D. L. Stewart
8470 R. L. Rinne
8471 A. C. Skinrood
8524 P. W. Dean